PNEUmorph: a shape-morphing interface comprising a pneumatic membrane constrained by variable-length tendons

Valentina Soana, Federico Bosi and Helge A. Wurdemann

***Abstract*— Soft shape-morphing technologies are explored in fields such as soft robotics, metamaterials and design, enabling systems to adapt dynamically through elastic deformations. Applied in mobile devices, actuators, interactive objects and environments, these systems can respond to functional needs and environmental stimuli, communicating information and enhancing human experiences. A primary design goal for these systems is achieving extensive and complex shape transformations. Traditionally, soft robotics employs a pneumatic active layer constrained by a passive layer, limiting the deformation range. However, using dual active layers can expand deformation potential. Expanding on these principles, this work introduces PNEUmorph: a pneumatic surface constrained by a network of variable-length tendons, allowing broader shape transformations than traditional single-layer systems. PNEUmorph's dual-layer actuation overcomes fixed deformation limits, significantly enhancing shape-morphing capabilities. This paper presents PNEUmorph's design and geometrical characterization, achieved through an interdisciplinary approach that merges design and soft robotics methods. This study details methods for simulation, fabrication, operation and evaluation, offering insights into experimental results and directions for advancing surface-based soft shape-morphing systems.**

I. INTRODUCTION

Soft shape-morphing technologies are being advanced in fields such as soft robotics [1], metamaterials [2] and design [3], creating systems that dynamically change shape through elastic material deformations. These innovations are used in mobile systems [4], actuators and interactive environments [5] that enhance daily life by responding to functional needs and environmental stimuli [6]. Such technologies align with the larger vision of integrating intelligent objects into everyday environments [7], allowing robotic systems to surpass traditional roles and interact seamlessly with humans [8]. Shape-morphing soft membranes, notable for their flexibility, lightweight properties, and ability to conform to complex geometries, undergo significant deformation with minimal material and actuation. This maintains structural integrity, making them ideal for various adaptive systems and design applications [9]. Unlike purely engineering-focused approaches, where shapes primarily fulfill functional needs, in design realms where aesthetics and other qualitative evaluations are crucial, the complexities of shape-morphing enhance the performance and functionality of systems. In engineering, particularly within soft robotics, the focus has traditionally been on developing control methods for elastic deformations tailored to small-scale, specific applications. Conversely, fields like architecture and structural design have long explored complex shapes of elastic systems, but often these built structures remain static due to technical limitations. The expansion of soft robotics and related engineering disciplines is now being driven by a multidisciplinary approach that has spurred the development of innovative shape-changing interfaces [10], [11] and the use of flexible materials [12], which enhance interaction with adaptive devices [13]. These technologies have been applied to create dynamic objects and environments to enhance daily activities [14], [15]. Despite these advances, the lack of unified design methodologies still challenges the achievement of complex shape changes and integrated control across various scales. Researchers are exploring large-scale, multistable soft systems [16] focusing on deployable structures induced by buckling [17], pneumatic actuation in origami structures [18], and planar patterned fabrics [19]. Projects such as Printflatables [20] integrate soft robotic principles into functional furniture designs [21], pushing the scaling of soft robotics to human sizes and merging design concepts with robotic techniques.

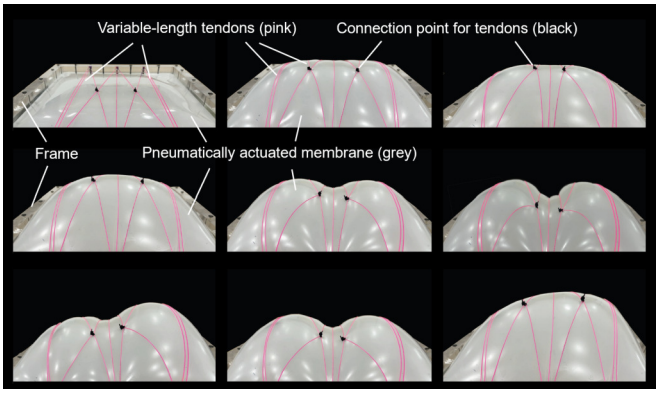

Fig. 1. Configuration examples of the PNEUmorph system: PNEUmorph is a shape-morphing interface composed of a pneumatically actuated membrane constrained by variable-length tendons. The subfigures illustrate representative deformations observed during experimental trials presented in Section III. The membrane can be inflated to varying internal pressures, while an overlaid tendon network modulates its shape. This network consists of three sets of three tendons, each arranged at equal intervals across the membrane. Tendons from one set are connected to their nearest counterparts in adjacent sets, forming either rectangular or diamond-like configurations. By altering tendon lengths and strain, the system imposes geometric constraints on the membrane, resulting in morphologies determined by the interplay between tendon architecture and pneumatic pressure.

This work has been supported by the Department of Mechanical Engineering at UCL.

V. Soana, F. Bosi and H.A. Wurdemann are with the Department of Mechanical Engineering, University College London, Torrington Place, London WC1E 7JE, United Kingdom. valentina.soana.18@ucl.ac.uk, f.bosi@ucl.ac.uk, h.wurdemann@ucl.ac.uk

Evaluating the performance of shape-morphing systems presents a complex challenge. Wang and Chortos highlight significant factors when assessing these systems, including the ability to achieve a substantial range of morphing possibilities, maximum deformation curvatures, and the variety of transformation patterns that a single prototype can exhibit [22]. Thus, the objective of designing a system capable of enabling a wide array of shapes should focus on achieving high limits of maximum change and a diverse array of transformation options, as well as significant curvature changes. In soft shape-morphing systems, specific shapes are achieved by regulating air pressure and selectively constraining membrane inflation. In soft robotics, an active layer (such as a pneumatic chamber) is typically constrained with a passive layer that limits deformation, defining the system's range of motion [23], [24], [25], [26]. Introducing two active layers can further extend deformation limits, though this approach has mostly been applied in tendon-driven soft actuators, such as grippers and cylindrical manipulators, where parallel tendons are integrated into small, cylindrical pneumatic chambers [28], [27]. In addition, soft robotic surfaces offer the potential to broaden applications to interactive interfaces and adaptable objects; however, they remain under explored with limited exceptions. While previous examples of shape-morphing surfaces predominantly relied on single-layer actuation, where shape transformations were inherently constrained by the passive layer's topology [29], more recent developments have explored systems with embedded tendons [30]. However, these systems still face limitations in adaptability and scalability. The integration of tendons within the surface can restrict the ability to modify patterns, limiting the range of achievable deformations. Additionally, fabrication complexity and predefined tendon arrangements impose constraints on scalability and versatility, particularly in applications requiring multiple shape transformations and a diverse network of tendons. Despite these advancements, challenges remain in precisely controlling and predicting complex deformations, highlighting the need for further development beyond the work presented here.

This work advances research on soft robotic surfaces and shape-morphing systems using two active layers through the development of PNEUmorph: a pneumatic membrane constrained by a network of variable-length tendons (see Fig. 1). The approach enables a wider range of shape transformations than conventional pneumatic systems, where deformation limits are fixed by the structure of the constraining layer. By enabling significant changes in the constraining layer surface limits can increase significantly. The system comprises a shape-morphing, soft-robotic material with a pneumatically actuated surface, which is constrained by a network of tendons with variable lengths. Our multidisciplinary approach contributes to the creation of shape-morphing systems capable of creating transformable environments. This vision encompasses furniture applications, such as interactive seating systems, as well as lightweight, adaptive building elements enhancing both functionality and user experience in responsive spaces.

Section II presents the design, fabrication, and simulation of PNEUmorph. Section III describes the experiments conducted and provides a characterization of PNEUmorph, including experimental results that present a geometric analysis of deformations based on modified actuation parameters. Section IV suggests directions for future research.

II. DESIGN, SIMULATION AND FABRICATION

The development of PNEUmoprh involved: 1) Design, fabrication and assembly of the physical setup; 2) Development of the robotic feedback-based actuation system and geometrical characterization methods; 3) Simulation studies; 4) Calibration procedures.

A. Design, fabrication, and assembly of the physical setup

The physical setup included a pneumatic membrane mounted on a base with an integrated chamber and a network of tendons on top. The system was designed to evaluate how variations in tendon lengths, patterns and pressure values affect membrane deformations (Fig. 2). The system featured a square membrane made of natural latex, measuring 300×300 mm^2, with a thickness of 0.08 mm and a Young's modulus of approximately 1 MPa.

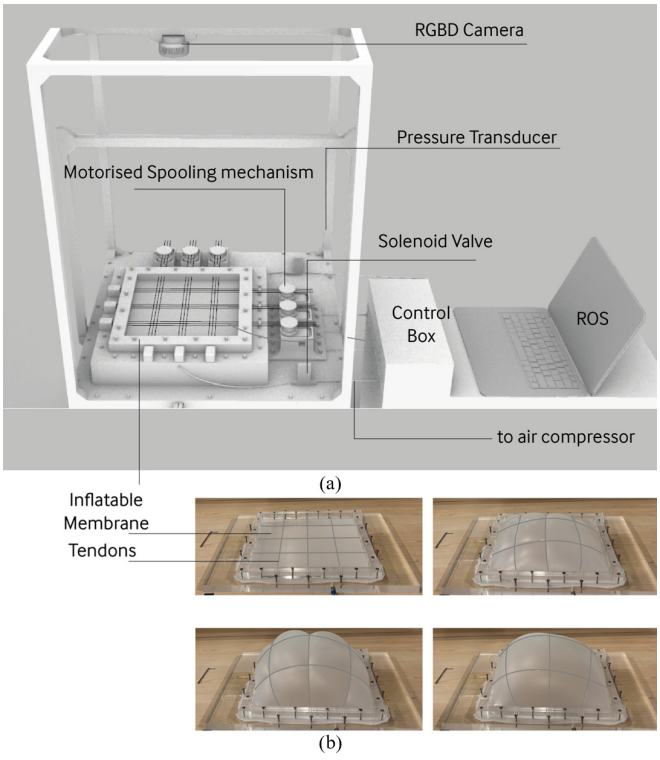

Fig. 2. The PNEUmorph physical setup: (a) The inflated membrane is secured to a base frame and constrained by a tendon architectural network. The pneumatic feedback system includes spooling mechanisms on both sides of the frame, an RGB-D camera positioned above the system, a pressure transducer, a solenoid valve, and the control system. Sensor data is processed to compute control values for the spooling mechanism, regulate the valve state, and generate a point cloud reconstruction of the membrane for geometrical analysis. (b) The inflated membrane can be constrained by, e.g., a grid-like tendon network arranged in a 3×3 grid.

The membrane was clamped between a square plexiglass frame and a corresponding base with an integrated chamber. It was positioned within the setup and inflated. The base was equipped with three pneumatic inlets for air intake, pressure sensing, and air release. A network of tendons, made of 1 mm diameter braided nylon cord, was positioned 1 cm above the membrane and arranged through custom holes on the frame sides. The main holes, 2 mm in diameter and spaced 7.5 mm apart, formed a 3×3 square tendon pattern, allowing different configurations within these fixed constraints. Additional 2 mm holes, placed 2 mm adjacent to each main hole, accommodated extra tendons. These tendons were anchored on one side of the frame and connected to motorized spools that adjusted their length.

The feedback-based actuation system used pressurized air to inflate the membrane and regulated its deformation by monitoring internal pressure in real-time. It included a camera system to track membrane deformation and capture data for geometric reconstruction, as well as motorized spools to adjust tendon lengths (Fig. 3). The initial feedback-actuation setup included a pressure regulation system using

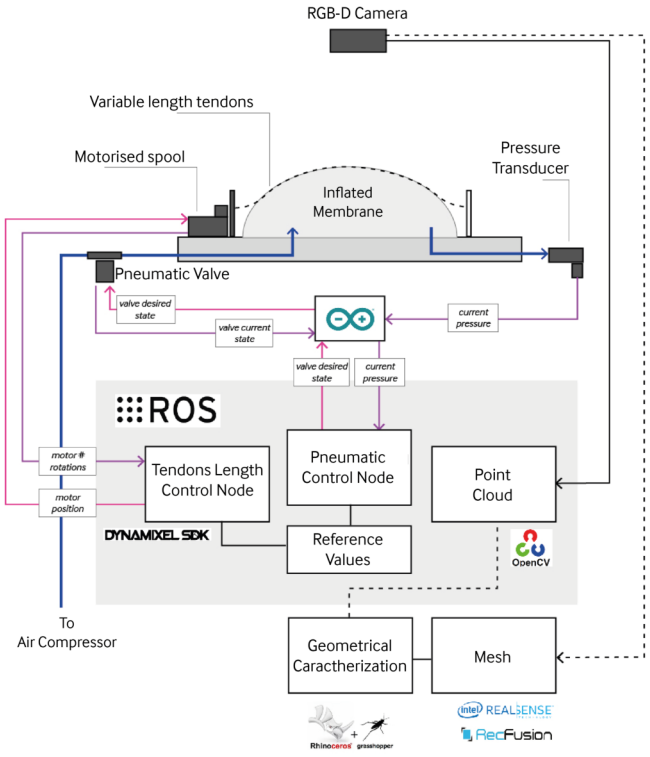

Fig. 3. The PNEUmorph robotic feedback-based actuation system utilizes pressurized air to inflate the membrane, a camera system to monitor deformations and collect data for geometry reconstruction, and motorized spools to adjust tendon length. The diagram illustrates the ROS control network, where real-time pressure data from the pressure transducer is collected and used to regulate the pneumatic valve and tendon lengths based on goal/reference values that define the desired actuation sequence. An RGB-D camera positioned above the system captures point cloud data in real-time at different actuation stages, storing it as PLY files for geometry reconstruction in Grasshopper. The integration of sensor data from motor positions, pressure readings, and the camera enables the geometrical characterization of the system under various conditions.

an RS Series ITV0000 pressure regulator, controlled by either an Arduino microcontroller or a National Instruments Data Acquisition (DAQ) system. Early tests, with digital image correlation camera capturing intervals using VICsnap software, indicated that internal pressures were below the range of commercial regulators. This led to the development of a custom pneumatic regulation system tailored for lower pressures, improving functionality and accuracy. The feedback-actuation setup utilized a custom pneumatic regulator system and an Intel RealSense L515 RGB-D camera. The pneumatic system included a Festo 2/2 Closed Monostable Solenoid Pilot Valve with a 6 mm MHJ Series electrical push-in (24 V DC, part number 567503, operating at a pressure range of 0.5 to 6 bar) and a pressure transducer with a 0.1 bar max range (RS PRO Pressure Sensor, Voltage Output, Relative Reading), both integrated with an Arduino. The solenoid valve, powered by a 24 V supply, had three connections: power, ground, and a digital control input from the Arduino, which sent signals to open (high, 5 V) or close (low, 0 V) the valve. The pressure transducer, also connected to the 24 V supply and ground, sent voltage variations to the Arduino's analogue input, allowing continuous pressure monitoring. Embedded Arduino control logic utilized real-time transducer data to regulate pressure to a set threshold. By converting voltage readings into pressure, the Arduino adjusted airflow through the valve to maintain desired pressure levels, proving essential for precise system functionality. The Intel RealSense L515 RGB-D camera was used to acquire geometric data and reconstruct the membrane's surface geometry. This was achieved using RealSense and RecFusion software in combination with custom Python scripts based on OpenCV. These scripts captured point cloud data at specific frames and saved it as PLY files, which were later imported into Rhinoceros/Grasshopper for analysis. The process involved importing the pyrealsense2, numpy, and cv2 libraries, configuring the RealSense pipeline, and streaming both depth and color data. Once stabilized, the system processed each frame by converting the color image to the HSV color space to isolate specific color ranges, improving depth filtering and reconstruction. The validated depth data was then used to generate a 3D point cloud focused on targeted regions. This method provided an effective integration of OpenCV and RealSense for accurate geometry capture and analysis within the Rhinoceros/Grasshopper environment.

The pneumatic system, motorized spooling control, and geometry reconstruction were integrated into ROS for streamlined communication and data processing. A rosserial Python node established a connection with the Arduino, enabling it to share sensor and valve data within the ROS network. Control algorithms for the Dynamixel MX-106 servo motor and RGB-D acquisition were converted to ROS nodes, supporting feedback-based control and seamless coordination across the pneumatic system, spooling mechanism, and camera via ROS topics. The motorized spool system used a spool mounted on a rotating shaft driven by a ROBOTIS Dynamixel MX-106 servo motor. Up to six motorized spools were positioned along the membrane

frame, each controlling a tendon routed through side holes and placed above the membrane to form a constraining layer. A custom 3D-printed case secured each spool to the base and connected it to the MX-106 output shaft, translating motor rotation into tendon movement. The system interfaced with a computer using a U2D2 adapter for communication and an SMPS2Dynamixel adapter for power (12-14.8 V). Python code utilising the Dynamixel SDK enabled control of the servo's position, speed and torque. The MX-106 provided a resolution of 0.088 degrees per unit and supported multiple rotations for extended tendon control. The feedback-based pneumatic system, motorised spooling control, and geometric reconstruction were integrated into ROS, enabling feedback-based control logic.

B. PNEUmorph Simulation

The simulation of PNEUmorph begins with the identification of the main design parameters and evaluation. The morphing capabilities of the system are influenced by three main design parameters: the geometry and material of the pneumatic membrane, the number, materials, and pattern of the tendon network and topology, and the actuation sequence. These elements collectively determine how effectively the system can adapt and change its shape. The primary evaluation of PNEUmorph is conducted through the geometric characterization of the system's deformations. The main objective is to facilitate complex alterations in the surface shapes with minimal changes in pressure and tendon lengths. The term complex in this context denotes deformations that include multiple curvatures and shifts in curvature, extending beyond basic bending or ballooning. The PNEUmorph design simulation process is conducted with numerical form-finding studies using the Kangaroo physics plugin for Grasshopper [31], calibrated with physical prototype. Kangaroo Physics is a live Physics engine software, able to simulate complex physical behavior, providing immediate feedback and iterative design possibilities. It uses discrete elements and a local stiffness-based solver where 'Goals' components set physical constraints with defined strength values to maintain system equilibrium. In simulations, the system's membranes and tendons are modeled as meshes and lines input into Length Goals components, which consider each element's material properties, rest-length, and strength. Strength is calculated using the formula EA/L, where E is Young's modulus (Pa), A is the cross-sectional area (m^2), and L is the rest length (m), and it determines the rigidity during simulations. The Pressure Goal dictates the main load conditions, while additional constraints like Anchor Points and Floor ensure structural stability under load. Custom Grasshopper scripts were developed to generate the membrane mesh and tendon pattern, which were inputted into Kangaroo using Length and Pressure Goals, alongside Anchor-point Loads and Floor Goals. The membrane's geometry was selected to a square shape to create a more versatile, surface-like system suitable for various applications including building envelopes and furniture. The system was simulated using different tendon length values (Fig. 4).

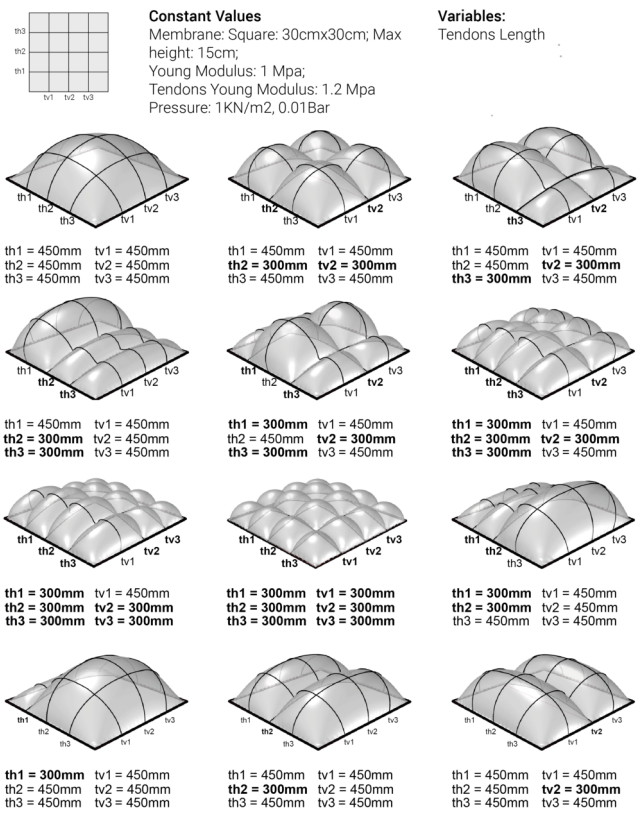

Fig. 4. PNEUmorph simulation using the Kangaroo Physics plugin for Grasshopper: The simulation of a pneumatic mesh constrained by a 3×3 network of variable-length tendons represents the elastic membrane inflated at 0.01 bar, with tendon lengths modified using the Kangaroo Length-Goal function. Each state corresponds to a different tendon length configuration, varying between 300 to 450 mm. The varying tendon lengths for each geometry are highlighted in bold. The simulation explores various geometrical states achieved by altering tendon lengths.

C. PNEUmorph calibration

The calibration phase began with the development and validation of the pneumatic actuation and motorized tendon systems. Initial tests established the pressure and tendon length ranges for stable membrane deformation. In calibration procedures 1 and 2 (Figs. 5a and 5b), the minimum and maximum pressure thresholds and actuation parameters were tuned to enable controlled shape changes. These results directly informed the design and control setup used in the subsequent geometrical reconstruction experiments.

In the first procedure (Fig. 5a), performed on a membrane without tendons, incremental pressure increases were applied to observe deformation, with significant inflation achieved up to 0.013 bar. The procedure was then repeated using a membrane constrained by parallel tendons of constant 310 mm length (Fig. 5b). After tests with three single tendons, the tendons were arranged in three groups of three. Each group was closely spaced to function as a single unit, and the groups were spaced apart to form a regular pattern dividing the membrane into four zones. This configuration provided enough stiffness for the nylon tendons to shape the membrane effectively during inflation without failure.

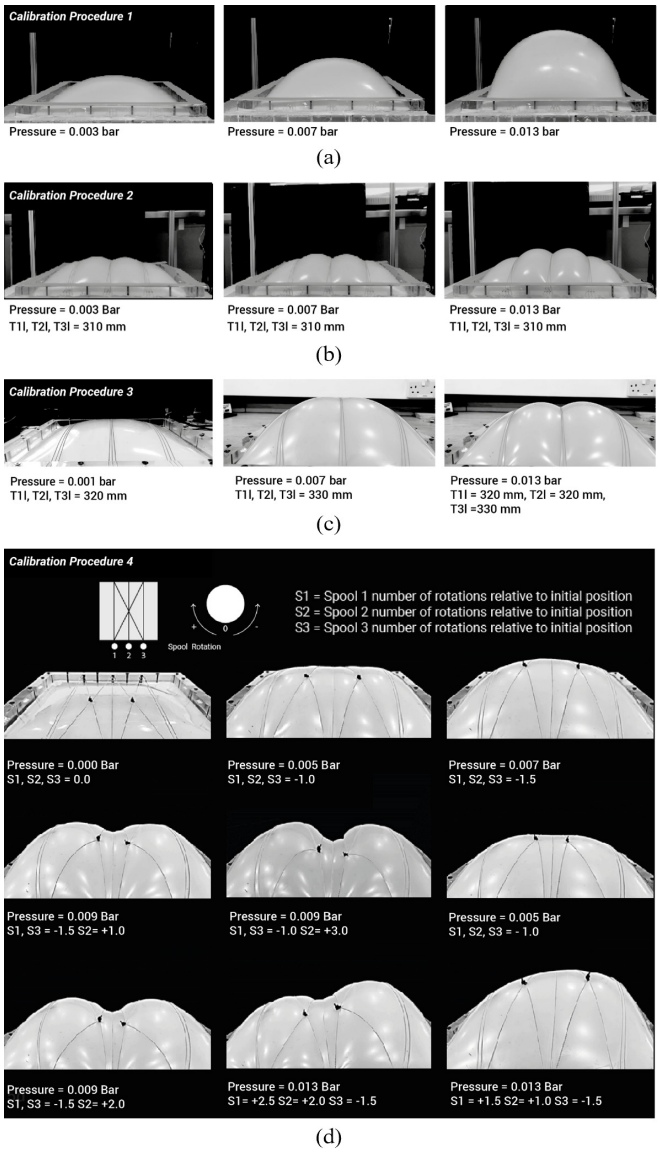

Fig. 5. The PNEUmorph Calibration procedures aim to understand 7 key actuation parameters for the experiments with a membrane inflated in different conditions: (a) The inflated membrane deformations were analyzed by identifying the minimum, maximum, and intermediate pressures required to deform the membrane. (b) The membrane is inflated and constrained by a network of nine parallel tendons of constant 310 mm length. (c) The tendon pattern on the inflated membrane is the same as in procedure 2, but the length of the tendons varies. (d) The tendon pattern differs from the previous configuration of three parallel groups of tendons. Now, one tendon from each group is connected to form a pattern transitioning from a line to a middle diamond shape, then to a diamond shape, and back to a line.

In this testing sequence, the operational states of a pneumatic membrane are sequentially examined. Initially, in state 1, the membrane is inflated to a pressure of 0.003 bar with tendon lengths set at 310 mm. Progressing to multiple states, the pressure within the membrane is increased to 0.007 and 0.13 bar while maintaining the tendon lengths unchanged. In calibration procedure 3 (Fig. 5c) the tendon pattern is the same as procedure 2, but the length of the tendons varies. In state 1, the membrane is inflated to a pressure of 0.001 bar, with the initial tendon lengths set to 320 mm. In state 2, the pressure is increased to 0.007 bar, while the tendon lengths are 330 mm. To elongate the tendons by 10 mm, reaching a total length of 330 mm, and given a spool diameter of 2 cm, the motor needs to rotate approximately 57.3 degrees. Therefore, the input to the Dynamixel goal position method in the control logic should set the Dynamixel MX-106 servo motor to a position value of approximately 653 to achieve this rotation. In state 3, the middle tendons are shortened back to the initial length of 320 mm. This demonstrates how the sequence of actuation and changes in tendon lengths cause variations in the system. In calibration procedure 4 (Fig. 5d), the tendon pattern differs from the previous configuration of three parallel groups of tendons. Instead, one tendon from each group is connected to form a pattern transitioning from a line to a middle diamond shape, then to a diamond shape, and back to a line. Specifically, the third tendon of tendon group 1 is connected in the middle with tendon 1 of group 2, and tendon 3 of group 2 is connected to tendon 1 of group 3. This new configuration creates a more complex and interconnected pattern without changing the overall tendon arrangement or number. Additionally, the length of the tendons varied at each state. This arrangement was designed to explore more complex deformations, test the mechanical capabilities of the spool mechanism, and customize the Dynamixel rotation control code. The objective was to observe how the goal positions set for the Dynamixel and the resultant number of rotations influenced tendon lengths and membrane deformation. Nine main states were identified by combining changes in pressure within the range of 0.00 bar to 0.013 bar and spool rotation for a maximum of three full rotations, both clockwise (to wind and shorten the tendons) and counterclockwise (to unwind and elongate the tendons). Data obtained during these procedures were used as a key reference for the geometrical characterization experiments presented in the next section.

III. EXPERIMENTAL RESULTS AND DISCUSSION

Six experiments were conducted to analyze the system's shape-changing capabilities by varying tendon pattern designs, lengths, and pneumatic actuation parameters to characterize its geometry. The experiments on geometrical reconstruction were conducted using the setup in Fig. 7, analyzing the shape of the membrane under varying tendon conditions: Experiments (E) 1 to 4 examined different numbers of tendons with constant length; E5 analyzed deformation with a network of three parallel tendons of variable length; E6 investigated the geometry of the membrane when restricted by a diamond-parallel tendon network with variable length.

A. Experiments 1 to 4 (E1, E2, E3 and E4)

1) E1, E2, E3 and E4 Protocol: Once the actuation system was configured using the outputs of the calibration procedures, the first four experiments focused on the geometric reconstruction of an inflated membrane constrained by different numbers of tendons of constant length.

E1 involved reconstructing the inflation behavior of the membrane without tendon constraints, serving as a baseline for evaluating height and section curves in later tendon-based experiments. E2 examined the membrane's deformation with a single central tendon of 300 mm in length, while E3 investigated a tendon network composed of three parallel tendons, each fixed at 300 mm. E4 analyzed the effects of a single central tendon extended to a length of 400 mm (Fig. 6a). E1-4 use the same protocol inflating the membrane at increments of 0.002 bar starting from 0.003 bar to 0.013 bar, and capturing and processing RGB-D data. A custom ROS package, Pneumatic-control-RGBD, was developed to simultaneously launch the pneumatic actuation and RGBD camera nodes. The pneumatic actuation node starts by opening the solenoid valve connected to the air compressor, which begins inflating the membrane. Once the pressure transmitter records the desired pressure value inside the membrane, the valve is turned off. This process is programmed for the desired increments up to 0.013 bar. After achieving the desired pressure, the valve closes for 60 seconds, during which the RGBD control node is activated to capture the frame at that pressure interval and save it as .ply files in a dedicated folder. Then, the valve reactivates until the next pressure increment is reached, and the process repeats. Upon the conclusion of the experiments, the.ply files are imported into Rhinoceros/Grasshopper, where a custom definition is developed to process these files, rebuild a mesh, perform a curvature analysis, and extract cross-sectional profiles along the central axis to create a graph visualizing the relationship between the pressure values and the maximum curvature at the center point of the membrane. Each experiment was repeated five times.

2) E1, E2, E3 and E4 Results: Across all experiments, deformations in the form of displacements of curvature points were observed in six pressure states, ranging from 0.003 bar to 0.013 bar with increments of 0.002 bar, based on reconstructions of the rebuilt geometry. The reconstructed surface of E1 (Fig. 6a) and its cross-section (Fig. 6c) show that the maximum height remained centrally located, with a non-linear displacement pattern: approximately 58 mm at state 1, increasing to 85 mm by state 3 (0.007 bar), and reaching 130 mm by state 6. This pattern suggests a rapid increase in displacement at lower pressures, with displacement reaching 130 mm as pressure approached 0.013 bar. Fig. 6b illustrates the relationship between the height of the maximum curvature point and pressure, based on six repetitions of the experiment, confirming the repeatability of these results. The reconstructed surface in Experiment 2 (Fig. 6d) and cross-section (Fig. 6f) reveal that the centrally positioned constant-length tendon constrained the membrane's deformation, anchoring the minimum curvature point at the center. Maximum curvature points emerged on either side of the membrane, shifting along the x, y, and z axes as pressure increased. Displacement of these maximum curvature points ranged from approximately 25 mm at state 1 to 65 mm at state 6, with an intermediate displacement of 40 mm at state 3. The minimum curvature

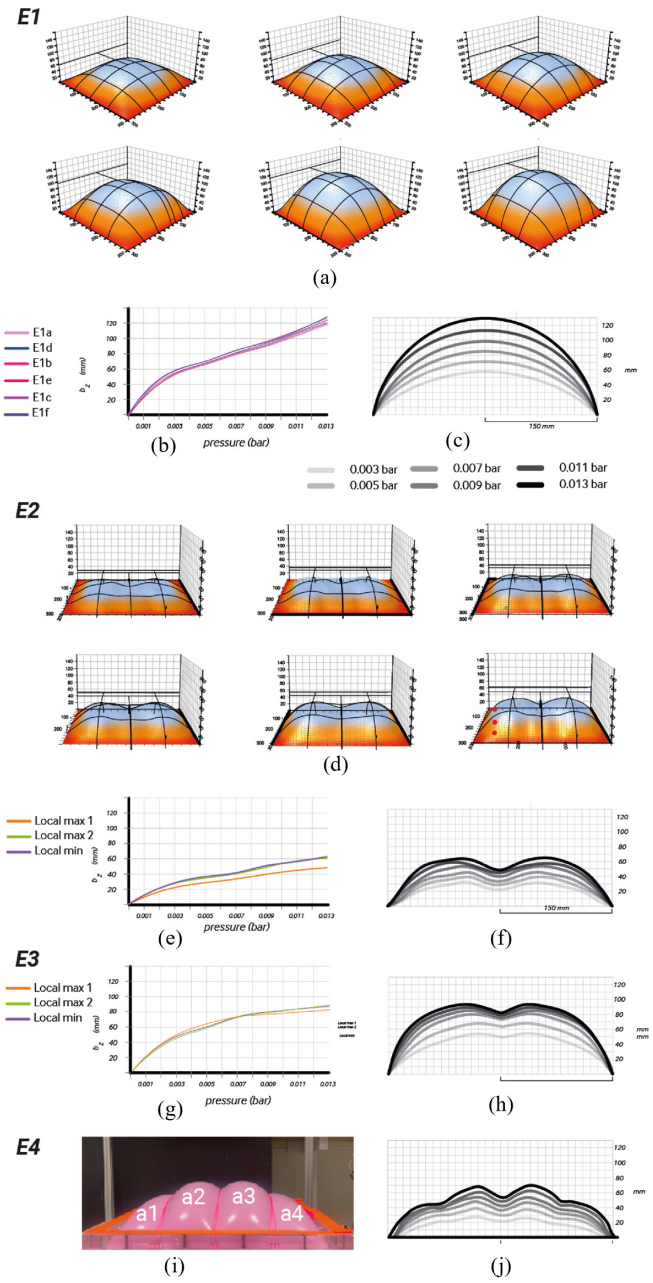

Fig. 6. The geometrical analysis and reconstruction from the RGBD camera from the four experiments focus on the geometrical reconstruction analysis of the membrane under varying tendon patterns but with a constant length. The subfigures show the reconstructed mesh, an analysis of the relationship between pressure and the minimum/maximum curvature of the rebuilt geometry, and cross-sectional views of the different conditions.

points also exhibited incremental displacement, from around 21 mm at state 1 to 50 mm at state 6, indicating that the tendon configuration limited overall deformation while allowing for controlled displacement under higher pressures. Fig. 6e shows the relationship between pressure and the height of the two local maxima and one local minimum point. In E3, the setup resembled E2 but with an elongated central tendon, allowing greater membrane deformation and yielding a middle ground between the behaviors seen in E1

and E2. From the cross section (Fig. 6h) it is possible to see that the minimum curvature point remained centered, with displacements of approximately 50 mm at state 1, 70 mm at state 3, and 80 mm at state 6. Maximum curvature values varied from about 55 mm to 95 mm across the pressure states (Fig. 6g), suggesting enhanced deformability compared to E2 but less than the unconstrained state of E1. E4 introduced three tendons (t1, t2, and t3), dividing the membrane into four areas (a1, a2, a3, and a4) as shown in Fig. 6i, and increasing shape complexity. Cross-sectional analysis in Fig. j revealed shifts in tendon and maximum curvature points within each area. In state 1, t1, t2, and t3 heights were approximately 30 mm, with maximum heights of around 25 mm in areas a1 and a4, and 35 mm in a2 and a3. In state 2, tendon heights varied, with t2 reaching 46 mm and t1 and t3 at 42 mm, while maximum heights rose to 44 mm for a1 and a4 and 55 mm for a2 and a3. By state 3, tendon heights further increased to 66 mm for t2 and 60 mm for t1 and t3, with maximum heights reaching 66 mm in a1 and a4, and 80 mm in a2 and a3. These results illustrate that the addition of three tendons in E4 created distinct deformation zones, with areas a2 and a3 consistently displaying greater deformation than a1 and a4, suggesting that tendon positioning and number can control localized membrane deformation.

B. Experiment 5 (E5)

1) E5 Protocol: E5 in Fig. 7a focused on exploring geometrical deformations and analyzing the inflated membrane constrained by a network of three parallel tendons. This experiment varies both the pressure and the length of the tendons to observe changes in the shape and curvature of the membrane. It utilizes the custom developed 'pneumatic-tendons-control-RGBD' ROS package, which extends the control logic of previous experiments by integrating the ability to control Dynamixel motor positions and consequently the spool's number of rotations. This functionality allows for the elongation and shortening of the tendons, as described in the calibration procedure 3. Each geometrical state is captured, rebuilt, and corresponds to a specific pressure value and tendon length. The experiment begins with an initial pressure of 0.011 bar and tendon lengths of 400 mm for the middle and 330 mm for the others (state 1). The spool system then rotates to shorten the tendons to 300 mm, resulting in a change of shape (state 2). The spool is subsequently unwound to the previous values (state 3). Next, the pressure increases to 0.015 bar while the tendons shorten again (state 4), then to 0.017 bar (state 5). The tendons elongate once more (state 6), then the pressure increases to 0.019 bar (state 7), and finally, the middle tendons shorten again (state 8).

2) E5 Results: From the geometrical reconstruction process, it can be observed how the sequence and variation of actuation values affect the membrane shape. States 1-3 showcase the same input pressure value of 0.011 bar, while the length of the tendons changes. Shortening the tendon length causes a change of the shape of the membrane as observed in the geometrical reconstruction. The middle point

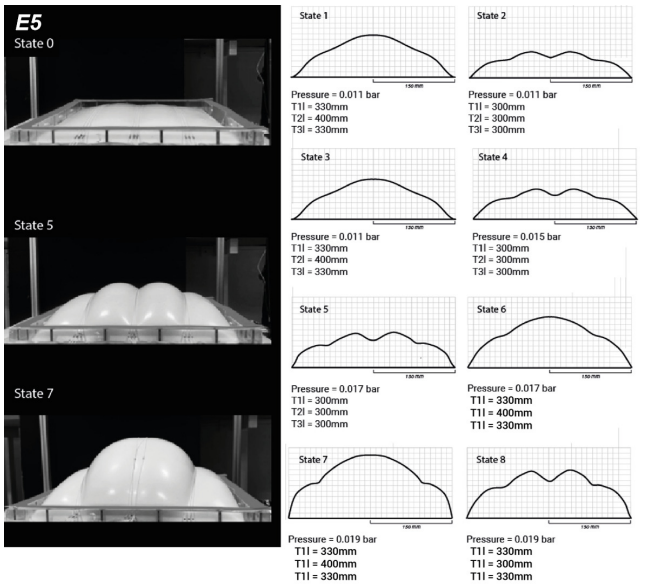

(a)

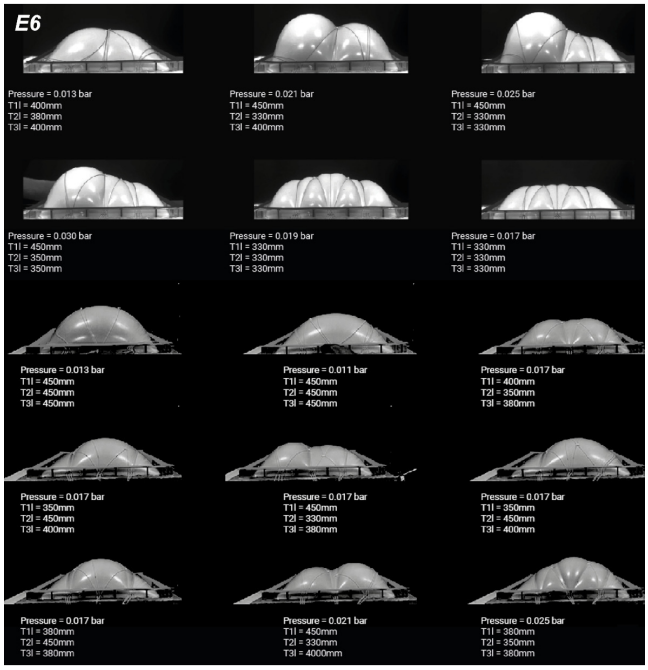

(b)

Fig. 7. (a) E5 focused on exploring geometrical deformations and analysing the inflated membrane constrained by a network of three parallel tendons. (b) E6 explored more complex tendon patterns, focusing on observing geometrical deformations of an inflated membrane constrained by a diamond-parallel pattern network of tendons with variable lengths.

which represents t2 corresponds to the max curvature value in states 1, 3, 6 and 7, while it decreases significantly in 2, 4, 5 and 8, where the change of length of the tendons created a visible deformation of the surface similar to E4.

C. Experiment 6 (E6)

1) E6 Protocol: E6 explores more complex tendon patterns, focusing on observing geometrical deformations of an inflated membrane constrained by a diamond-parallel pattern

network of tendons with variable lengths (Fig. 7b). It can be observed that the diamond-parallel pattern network consists of nine tendons, however, only three spools are used to change the length of the network and generate significant deformations in combination with changes in pressure. Given the complex tendon pattern, which applies constraining pressure on the system, the pneumatic values required to inflate the membrane are higher, starting from 0.013 bar to values of 0.030 bar. These experiments have the same protocol as previous ones, with the difference that the motor values are manually controlled from the terminal. Once the system achieves the desired pneumatic values, motor position can be updated to achieve the desired tendon length.

2) E6 Results: From these preliminary complex shapes explorations many different states and significant changes in curvature can be observed throughout the images captured at different stages. This serves as a starting point to create and observe the varied changes and potential of the system.

D. Discussion

The results demonstrate the potential of PNEUmorph's dual active-layer system for complex shape-morphing, where small actuation variations significantly influence transformations. Experiments 2 and 3 show that a single tendon can generate over 20 deformation states. Experiment 5 reveals that actuation sequence impacts system morphology, while Experiment 4 illustrates how additional tendons increase the curvature complexity of deformation states. Experiment 6 suggests that intersecting constraints introduce new deformation modes, expanding the system's shape-morphing capabilities to achieve more complex shapes.

IV. Conclusion

This work represents an initial step toward developing adaptive surfaces with controlled shape-morphing capabilities for medium to large scale applications. The experiments highlight both the potential and challenges of predicting deformation, as complexity increases with additional parameters. Physical variability such as tendon friction, unintended movement, and mechanical constraints can disrupt symmetry and affect control, making adaptable strategies essential. Future work will focus on integrating closed loop control and real-time simulation within the ROS environment to improve precision and enable feedback-driven deformation. While these developments aim to enhance accuracy, the system is intended for creative applications where a higher tolerance for variability is acceptable compared to traditional task-specific soft robotics, and can even contribute to expressive outcomes. Embedding this membrane system into everyday surfaces (e.g., tables, chairs, walls) offers new possibilities for interactive environments where structure, responsiveness, and communication converge in tangible and engaging ways.

References

[1] D. Rus, M.T. Tolley, "Design, fabrication and control of soft robots," Nature, vol. 521, no. 7553, pp. 467-475, 2015.

[2] K. Bertoldi et al., "Flexible mechanical metamaterials," Nature Reviews Materials, vol. 2, no. 11, pp. 1-11, 2017.

[3] M. Wihart, The architecture of soft machines, Doctoral dissertation, UCL (University College London), 2015.

[4] Y. Sun et al., "Soft mobile robots: A review of soft robotic locomotion modes," Current Robotics Reports, vol. 2, pp. 371-397, 2021.

[5] B. Farahi, N. Leach, Eds., "Interactive Design: Towards a Responsive Environment," Basel: Birkhäuser, 2023.

[6] M. Coelho, J. Zigelbaum, "Shape-changing interfaces," Personal and Ubiquitous Computing, vol. 15, pp. 161-173, 2011.

[7] H. Bier et al., "Robotic building as integration of design-to-robotic-production and -operation," Robotic Building, pp. 97-120, 2018.

[8] V. Soana et al., "Elastic robotic structures: a multidisciplinary framework for the design and control of shape-morphing elastic system for architectural and design applications," Constr. Robot., vol. 9(3), 2025.

[9] I. Poupyrev, T. Nashida, M. Okabe, "Actuation and tangible user interfaces: the Vaucanson duck, robots, and shape displays," Tangible and Embedded Interaction, pp. 205-212, 2007.

[10] Y.K. Lee et al., "Recent progress in shape-transformable materials and their applications," Electronic Materials Letters, vol. 18, no. 3, pp. 215-231, 2022.

[11] J. Ou et al., "aeroMorph—heat-sealing inflatable shape-change materials for interaction design," User Interface Software and Technology, pp. 121-132, 2016.

[12] S. Follmer et al., "inFORM: dynamic physical affordances and constraints through shape and object actuation," User Interface Software and Technology, vol. 13, no. 10, pp. 2501-988, 2013.

[13] J. Alexander et al., "Grand challenges in shape-changing interface research," Human Factors in Computing Systems, pp. 1-14, 2018.

[14] K.Y. Choi et al., "Aspire: clippable, mobile pneumatic-haptic device for breathing rate regulation via personalizable tactile feedback," Human Factors in Comput. Syst., pp. 1-8, 2021.

[15] Y. Gaffary, A. Lécuyer, "The use of haptic and tactile information in the car to improve driving safety: A review of current technologies," Frontiers in ICT, vol. 5, no. 5, 2018.

[16] N.S. Usevitch et al., "An untethered isoperimetric soft robot," Science Robotics, vol. 5, no. 40, pp. eaaz0492, 2020.

[17] S. Mhatre et al., "Deployable structures based on buckling of curved beams upon a rotational input," Advanced Functional Materials, vol. 31, no. 35, pp. 2101144, 2021.

[18] D. Melancon et al., "Multistable inflatable origami structures at the metre scale," Nature, vol. 592, no. 7855, pp. 545-550, Apr. 22, 2021.

[19] E. Siéfert et al., "Programming stiff inflatable shells from planar patterned fabrics," Soft Matter, vol. 16, no. 34, pp. 7898-7903, 2020.

[20] H. Sareen et al., "Printflatables: printing human-scale, functional and dynamic inflatable objects," Conf. Human Factors in Computing Systems, pp. 3669-3680, 2017.

[21] E. Grönvall et al., "Causing commotion with a shape-changing bench: experiencing shape-changing interfaces in use," Human Factors in Computing Systems, pp. 2559-2568, 2014.

[22] J. Wang, A. Chortos, "Performance metrics for shape-morphing devices," Nature Reviews Materials, pp. 1-14, 2024.

[23] M. Manti, V. Cacucciolo, M. Cianchetti, "Stiffening in soft robotics: A review of the state of the art," IEEE Robotics & Automation Magazine, vol. 23, no. 3, pp. 93-106, 2016.

[24] J.M. Gandarias et al., "Open-loop position control in collaborative, modular variable-stiffness-link (VSL) robots," IEEE Robotics and Automation Letters, vol. 5, no. 2, pp. 1772-1779, 2020.

[25] J. Shi et al., "Design and characterisation of cross-sectional geometries for soft robotic manipulators with fibre-reinforced chambers," International Conference on Soft Robotics, pp. 157-164, 2022.

[26] J. Shi et al., "Miniaturised Soft Manipulators with Reinforced Actuation Chambers on the Sub-Centimetre Scale," International Conference on Soft Robotics, pp. 157-164, 2024.

[27] Wurdemann et al., "Antagonistic Actuation Technique for Simultaneous Stiffness and Position Control," International Conference on Intelligent Robotics and Applications, pp. 164-174, 2015.

[28] A. A. Stanley, A.M. Okamura, "Deformable model-based methods for shape control of a haptic jamming surface," IEEE Trans. Visualization Comput. Graphics, vol. 23, no. 2, pp. 1029-1041, 2016.

[29] A. Sciortino et al., "Active membrane deformations of a minimal synthetic cell," Nat. Phys., vol. 21, pp. 799–807, 2025.

[30] N. Sholl, K. Mohseni, "High-stretch, tendon-driven, fiber-reinforced membrane soft actuators with multiple active degrees of freedom," Communications Engineering, vol. 3, no. 1, p. 25, 2024.

[31] D. Piker, "Kangaroo: Physics-based simulation for Grasshopper," [Online]. Available: http://kangaroo3d.com/. [Accessed: Oct. 2024].